J. Fluid Mech. (2008), *vol.* 613, *pp.* 255–274.
doi:10.1017/S0022112008003248 Printed in the United Kingdom

Transition in pipe flow: the saddle structure on the boundary of turbulence

Y. DUGUET†, A. P. WILLIS‡
AND R. R. KERSWELL

School of Mathematics, University of Bristol, Bristol BS8 1TW, UK

(Received 14 November 2007 and in revised form 22 June 2008)

The laminar–turbulent boundary Σ is the set separating initial conditions which relaminarize uneventfully from those which become turbulent. Phase space trajectories on this hypersurface in cylindrical pipe flow appear to be chaotic and show recurring evidence of coherent structures. A general numerical technique is developed for recognizing approaches to these structures and then for identifying the exact coherent solutions themselves. Numerical evidence is presented which suggests that trajectories on Σ are organized around only a few travelling waves and their heteroclinic connections. If the flow is suitably constrained to a subspace with a discrete rotational symmetry, it is possible to find locally attracting travelling waves embedded within Σ. Four new types of travelling waves were found using this approach.

1. Introduction

Transition to turbulence in cylindrical pipe flow is governed by one single dimensionless parameter, the Reynolds number $Re := UD/\nu$ where U is the mean flow speed along the pipe, D the pipe diameter and ν the kinematic viscosity of the fluid (Reynolds 1883). Despite the simplicity of the setup, the reason for transition remains obscure due to the linear stability of the laminar Hagen–Poiseuille flow (Hagen 1839; Poiseuille 1840) and the sensitivity of the process to the exact shape and amplitude of disturbances present. In most experiments, transition is observed at $Re \sim 2000$ (e.g. Wygnanski & Champagne 1973) but can be triggered as low as $Re = 1750$ (Peixinho & Mullin 2006) or delayed to $Re = 100,000$ in very carefully controlled experiments (Pfenniger 1961). Until recently, the only firm theoretical result was the energy stability bound of $Re = 81.49$ (Joseph & Carmi 1969) below which *all* disturbances are guaranteed to decay monotonically. This is, however, more than an order of magnitude below the observed value for transition.

An important step forward in understanding the transition process was the discovery of disconnected solutions to the Navier–Stokes equations in a cylindrical pipe (Faisst & Eckhardt 2003; Wedin & Kerswell 2004; Kerswell 2005; Pringle & Kerswell 2007). These exact solutions are travelling waves (TWs) which appear through saddle-node bifurcations as in other shear flows (Nagata 1990; Waleffe 1997, 1998, 2001, 2003). All these solutions are linearly unstable though they have a very low-dimensional unstable manifold. There is much interest in these solutions, as very similar structures have been observed transiently in experiments (Hof *et al.* 2004, 2005) and direct numerical

† Present address: Linné Flow Centre, KTH Mechanics, SE-100 44 Stockholm, Sweden.
‡ Present address: Laboratoire d'Hydrodynamique, Ecole Polytechnique, 91128 Palaiseau, France.

simulations (Kerswell & Tutty 2007; Schneider, Eckhardt & Vollmer 2007*a*; Willis & Kerswell 2008*a*). These states can generally be divided into 'upper-branch' and 'lower-branch' TWs, based on whether they have high or low wall shear stress. Lower-branch solutions are believed to sit on a hypersurface that divides phase space into two regions: one where initial points lead directly to the laminar state, the other where initial conditions lead to turbulent episodes (Kawahara 2005; Wang, Gibson & Waleffe 2007; Kerswell & Tutty 2007; Viswanath 2008). The simple translational behaviour of these travelling wave solutions is inherent to the method used to find them, and undoubtedly masks an even larger variety of more complex exact solutions.

The boundary between laminar and turbulent trajectories – labelled Σ hereafter – is formally a separatrix if the turbulent state is an attractor. At low *Re*, however, turbulence may ultimately decay after a long transient, in which case the laminar state is the unique global attractor. Then the boundary Σ is generalized to the dividing set in phase space between trajectories which smoothly relaminarize and those which undergo turbulent evolution. Σ is thought to be of codimension 1 in phase space but one can *a priori* not exclude a more complex fractal structure, as suggested by the dependence of lifetime on initial conditions in simulations of pipe flow (Faisst & Eckhardt 2004). Trajectories which start in Σ – hereafter called the 'edge', following Skufca, Yorke & Eckhardt (2006) – stay in Σ for later times by definition and hence the long-time dynamics are of obvious interest. The long-time behaviour on Σ has already been found to be a periodic solution in plane Poiseuille flow in a pioneering study by Toh & Itano (1999); see also Itano & Toh (2001). Skufca *et al.* (2006) studied a nine-dimensional model of plane Couette flow (PCF) to reveal an attracting periodic orbit at low *Re* and an apparently chaotic state at higher *Re*. However, recent fully resolved simulations have shown that the asymptotic behaviour is an attracting TW in PCF (Schneider *et al.* 2008; Viswanath 2008) and a chaotic attractor in a short cylindrical pipe of length $L = 5D$ (Schneider, Eckhardt & Yorke 2007*b*). Interestingly, this seemingly chaotic end state looks to be centred around an 'asymmetric' TW (Pringle & Kerswell 2007; Mellibovsky & Meseguer 2007).

The purpose of this paper is to explore the dividing hypersurface Σ in pipe flow with the following objectives:

(*a*) to establish that the dynamics restricted to this laminar–turbulent boundary explores many different saddle points embedded in it;

(*b*) to find evidence for heteroclinic or 'relative' homoclinic connections between these saddle points;

(*c*) to explore Σ restricted by a discrete rotational symmetry in order to ascertain whether the limiting behaviour remains chaotic or can be a simple attractor;

(*d*) to develop a practical and general way to find TWs and periodic orbits without detailed knowledge of their spatial structure.

The works cited above employ a reduced computational domain for their calculations, imposing short-wavelength periodicity in one direction (along the pipe: Schneider *et al.* 2007*b*) or two (in the spanwise and streamwise directions in plane Couette flow: Schneider *et al.* 2008; Viswanath 2008). This is very much in the spirit of the Minimal Flow Unit pioneered by Jiménez & Moin (1991) and used with considerable success to identify key mechanisms underpinning turbulence (Hamilton, Kim & Waleffe 1995). In this paper, we also adopt this same approach by concentrating on pipes up to $5D$ long. The ensuing reduction in the degrees of freedom of the flow allows a much more detailed exploration of the flow dynamics, albeit restricted to a subspace of strict spatial periodicity. This is a necessary preliminary to

motivating a more carefully focused study in much longer pipes which can capture spatially localized turbulent structures (e.g. Priymak & Miyazaki 2004; Willis & Kerswell 2007, 2008*a*) but still at considerable numerical cost. Flow structures found in the short pipes considered here also exist, of course, in a longer pipe, but will be more unstable due to the greater degrees of freedom present there. It is also worth remarking that a recent study (Nikitin 2007) has shown how pipe flow is slow to lose its spatial periodicity when this restriction is lifted.

This paper is organized as follows. Section 2 discusses the formulation and numerical methods used to simulate the flow in a pipe and to extract exact recurrent flow solutions. Section 3 presents the results obtained using these in 7 subsections: § 3.1 recalls the method used to follow trajectories on Σ and confirms that the limiting behaviour looks chaotic (Schneider *et al.* 2007*b*); § 3.2 and § 3.3 discuss how near-recurrent states are identified, and using a Newton–Krylov algorithm demonstrate that a number of unstable travelling waves are approached; § 3.4 offers evidence for the existence of a 'relative' homoclinic connection between a travelling wave and the same wave rotated; § 3.5 looks for recurrent flow structures in Σ restricted by a discrete rotational symmetry and identifies new exact travelling wave solutions; § 3.6 shows that within this subspace the limiting state of Σ is a simple attractor; § 3.7 confirms that all the TWs found in the earlier subsections are indeed embedded in the laminar-turbulent boundary. The paper ends with a discussion in § 4.

2. Numerical procedure

2.1. *Governing equations*

We consider the incompressible flow of Newtonian fluid in a cylindrical pipe and adopt the usual set of cylindrical coordinates (s, θ, z) and velocity components $\boldsymbol{u} = u\hat{\boldsymbol{s}} + v\hat{\boldsymbol{\theta}} + w\hat{\boldsymbol{z}}$. The domain considered here is $(s, \theta, z) \in [0:1] \times [0:2\pi] \times [0:L]$, where $L = 2\pi/\alpha$ is the length of the pipe and lengths are in units of radii $(D/2)$. The flow is described by the incompressible three-dimensional Navier–Stokes equations

$$\frac{\partial \boldsymbol{u}}{\partial t} + (\boldsymbol{u}\cdot\nabla)\,\boldsymbol{u} = -\nabla p + \frac{1}{Re}\nabla^2\boldsymbol{u}, \tag{2.1}$$

$$\nabla\cdot\boldsymbol{u} = 0. \tag{2.2}$$

The flow is driven by a constant mass-flux condition, as in recent experiments (e.g. Peixinho & Mullin 2006). The boundary conditions are periodicity across the pipe length $\boldsymbol{u}(s, \theta, z) = \boldsymbol{u}(s, \theta, z + L)$ and no-slip on the walls $\boldsymbol{u}(1, \theta, z) = \boldsymbol{0}$.

2.2. *Time-stepping code*

The basic tool for the numerical determination of exact recurrent states is the accurate time-stepping code used by Willis & Kerswell (2007, 2008*a*). The velocity field is derived from two scalar potentials Ψ and Φ,

$$\boldsymbol{u} = \nabla\times(\Psi\hat{\boldsymbol{z}}) + \nabla\times\nabla\times(\Phi\hat{\boldsymbol{z}}), \tag{2.3}$$

and the incompressible Navier–Stokes equations are rewritten using the formulation introduced by Marqués (1990). The two scalar potentials are discretized using high-order finite differences in the radial direction s and spectral Fourier expansions in the azimuthal direction θ and axial direction z. For example, the decomposition of the

scalar potential Φ at a radial location s_j, $(j = 1, \ldots, N)$, reads

$$\Phi(s_j, \theta, z, t; \alpha, m_0) = \sum_{k=-K}^{K} \sum_{m=-M}^{M} \Phi_{jkm}(t) \mathrm{e}^{\mathrm{i}(m_0 m\theta + \alpha k z)}. \tag{2.4}$$

The positive integer m_0 refers to the discrete rotational symmetry

$$\boldsymbol{R}_{m_0} : (u, v, w, p)(s, \theta, z) \to (u, v, w, p)\left(s, \theta + \frac{2\pi}{m_0}, z\right) \tag{2.5}$$

of the flow (trivially $m_0 = 1$ means no rotational symmetry is imposed). The resolution of a given calculation is described by a vector (N, M, K). It is adjusted until the energy in the spectral coefficients drops by at least 5 and usually 6 decades from lowest- to highest-order modes. The time-stepping is second-order accurate with Δt updated using an adaptive method based on a CFL condition.

The number of (real) degrees of freedom, which defines the dimension of phase space, is $O(8MNK)$. The set of all complex coefficients $\boldsymbol{X} = \{\Phi_{jkm}, \Psi_{jkm}\}$ defines our phase space with its usual Euclidean norm $|\boldsymbol{X}| = \sqrt{\boldsymbol{X} \cdot \boldsymbol{X}}$. Symmetries exhibited by TWs such as the shift-and-reflect symmetry,

$$\boldsymbol{S} : (u, v, w, p)(s, \theta, z) \to (u, -v, w, p)\left(s, -\theta, z + \frac{\pi}{\alpha}\right), \tag{2.6}$$

and the mirror symmetry (e.g. Pringle & Kerswell 2007; Pringle, Duguet & Kerswell 2008),

$$\boldsymbol{Z} : (u, v, w, p)(s, \theta, z) \to (u, -v, w, p)(s, -\theta, z), \tag{2.7}$$

are not imposed in the simulations.

2.3. *The Newton–Krylov method*

The spectral expansion defined above converts the Navier–Stokes equations into an autonomous dynamical system of the form

$$\frac{\mathrm{d}\boldsymbol{X}}{\mathrm{d}t} = \boldsymbol{F}(\boldsymbol{X}). \tag{2.8}$$

Travelling wave solutions are 'relative equilibrium' solutions of the Navier–Stokes equations, steady in an appropriate Galilean frame. It is numerically convenient to seek and interpret them as a special case of 'relative periodic orbit' (RPO) (Viswanath 2007, 2008). We hence developed an algorithm to look for RPOs defined as zeros of the functional

$$g = |\boldsymbol{X}(T)^{-\Delta z, -\Delta\theta} - \boldsymbol{X}(0)|^2. \tag{2.9}$$

Here, $\boldsymbol{X}(T)$ is the point at time T on the trajectory starting at time $t = 0$ from the point $\boldsymbol{X}(0)$. $\boldsymbol{X}^{-\Delta z, -\Delta\theta}$ is the point in phase space corresponding to the state $\boldsymbol{X}$ shifted back in space by the distance Δz in the axial direction and by the angle $\Delta\theta$ in the azimuthal direction. A shift by $(\Delta z, \Delta\theta)$ corresponds in phase space to the transformation

$$(\Psi_{jkm}, \Phi_{jkm})\mathrm{e}^{-\mathrm{i}(m m_0 \Delta\theta + \alpha k \Delta z)} \to (\Psi_{jkm}, \Phi_{jkm}). \tag{2.10}$$

A zero of g corresponds to a flow repeating itself exactly after a time T, but at a different location defined by Δz and $\Delta\theta$. A travelling wave solution is an RPO where there is a degeneracy between the shifts Δz and $\Delta\theta$, and the period T. For the case of a TW propagating axially with speed c, $\Delta z = cT$, where T is an apparent period. To

remove this degeneracy, we impose $\Delta z = L$ unless otherwise specified. As the majority of known TWs do not rotate, $\Delta\theta = 0$ is also assumed (those that do rotate do so rather slowly: Pringle & Kerswell 2007). Starting from a good initial guess for $\boldsymbol{X}(0)$ and an estimate of the period T (to be discussed in § 3.2), we minimize the residual g using a Newton–Krylov algorithm, based on a GMRES algorithm (Saad & Schultz 1986). The size of the dynamical system (typically 10^5 degrees of freedom) necessitates the use of a matrix-free formulation. The use of an *inexact* Krylov solver also leads to a significant gain in computation time (we used choice 2 in Eisenstat & Walker 1996). Moreover, we embed the Newton solver into a more globally convergent strategy in order to improve likeliness of convergence, using a double dogleg step technique (Dennis & Schnabel 1995; Brown & Saad 1990). For the special case of TWs with a short period, we assume full convergence when the normalized residual $\sqrt{g}/|\boldsymbol{X}(0)|$ is less than $O(10^{-10})$.

2.4. *Stability of travelling waves*

Once a travelling wave solution is known, along with its axial propagation speed c, it can be expressed as a steady solution in the frame moving at speed c. In this Galilean frame, the stability of the solutions can be studied numerically using an eigenvalue solver based on an Arnoldi algorithm. This yields the leading eigenvalues whose real part, when positive, indicates the growth rate of infinitesimal perturbations to the exact solution in the moving frame.

3. Results

We present four 'edge' calculations, each motivated by a different question. In the first (see § 3.1–3.3), the edge in a pipe length $L \approx 5D$ ($\alpha = 0.625$) is calculated starting from a typical turbulent initial condition in order to investigate whether there are coherent structures buried in it. We are able to confirm the presence of what looks to be a chaotic attractor as found recently by Schneider *et al.* (2007*b*). In the second edge calculation (§ 3.4) we look for numerical evidence of heteroclinic connections between saddle points by using a perturbed TW as an initial condition. In the third (§ 3.5) we impose the discrete rotational symmetry $\boldsymbol{R}_2$ on the flow to exploit the saddle structure of the subset of Σ to reveal new TWs which possess $\boldsymbol{R}_2$-symmetry. In the fourth (§ 3.6) we look for evidence of multiple attracting TWs to demonstrate that under a rotational symmetry constraint the large-time dynamics need not be chaotic.

3.1. *Calculating edge trajectories*

In this subsection we choose a pipe with $\alpha = 0.625$ ($L = 5.0265D$) and $Re = 2875$, set $m_0 = 1$ so that there is no restriction on the rotational symmetry, and take a numerical resolution of (30, 15, 15). For this value of Re, turbulence, when triggered, is sustained over the typical simulation time which is much longer that the time taken to relaminarize. In order to constrain a numerical trajectory to stay on the edge surface, Σ, we use a shooting method analogous to that first used in plane Couette flow by Toh & Itano (1999). We first produce a long turbulent trajectory and pick a state $\boldsymbol{u}^*$ of relatively low three-dimensional disturbance energy $E_{3d}(t)$ (defined as the kinetic energy in the streamwise-dependent Fourier modes $k \neq 0$). Initial states are then chosen from the line,

$$\boldsymbol{u}_\beta := \langle\, \boldsymbol{u}^* \rangle + \beta(\boldsymbol{u}^* - \langle \boldsymbol{u}^* \rangle), \tag{3.1}$$

parametrized by the real number β and $\langle \quad \rangle := \alpha/(2\pi) \int_0^{2\pi/\alpha} (..)\, \mathrm{d}z$ is an axial average. The initial condition $\boldsymbol{u}_{\beta=0}$ is two-dimensional and hence does not trigger turbulence,

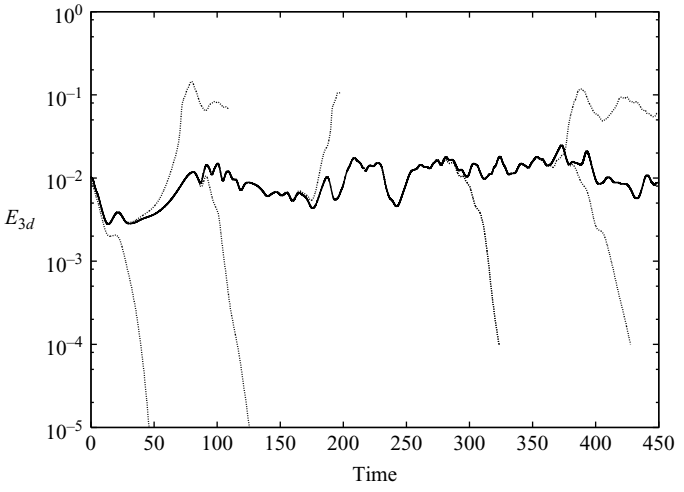

FIGURE 1. Energy contained in the axially dependent modes for $(\alpha, Re, m_0) = (0.625, 2875, 1)$. The thick line indicates the edge trajectory and the thinner lines nearby trajectories which either relaminarize (energy decreases) or become turbulent (energy increases to a higher level). Time is in units of D/U.

whereas $\boldsymbol{u}_{\beta=1}$ is the original turbulent state. This β-interval is then repeatedly halved with, at each stage, the new interval selected such that an initial condition corresponding to β at the lower limit relaminarizes, whereas that at the upper limit leads to large turbulent values of E_{3d}. β is refined close to machine accuracy using double-precision arithmetic, forcing the energy of the trajectory to stay at an intermediate level corresponding to the laminar–turbulent boundary for typical times of $O(200D/U)$. At the values of Re used here, the energy of this boundary is clearly distinct from those associated with turbulence and thus makes determination of β unambiguous. Once machine precision has been reached, the process is restarted from nearby states towards the end of the trajectory originating from neighbouring β values.

The full trajectory, of duration $O(500D/U)$, does not show any sign of convergence towards a simple state but rather displays erratic and unpredictable dynamics, as found by Schneider *et al.* (2007*b*). We deliberately avoid the word 'turbulent' as this refers to larger values of E_{3d}. Figure 1 shows the time evolution of the $E_{3d}(t)$.

3.2. *Near-recurrences on an edge trajectory*

Despite the lack of regularity of the energy signals, inspection of all velocity components at several random locations in the pipe indicate clearly that the flow on Σ is sometimes nearly periodic in time on short intervals. For the case $(\alpha, Re, m_0) = (0.625, 2875, 1)$, it is possible by eye to identify several temporal windows where all velocity components approximately oscillate with a given frequency (see figure 2). Within these windows the dynamics on the edge appear to be temporally correlated with a short period. A large number of snapshots were taken at times t_i, $i = 1, 2, 3\ldots$ across the whole trajectory. To investigate the possibility of recurrence in the flow, each snapshot state $\boldsymbol{X}(t_i)$ was used as an initial condition for time-stepping. The normalized distance in phase space between this initial point and its evolution in time was then examined for local minima. Specifically, we define the scalar residual

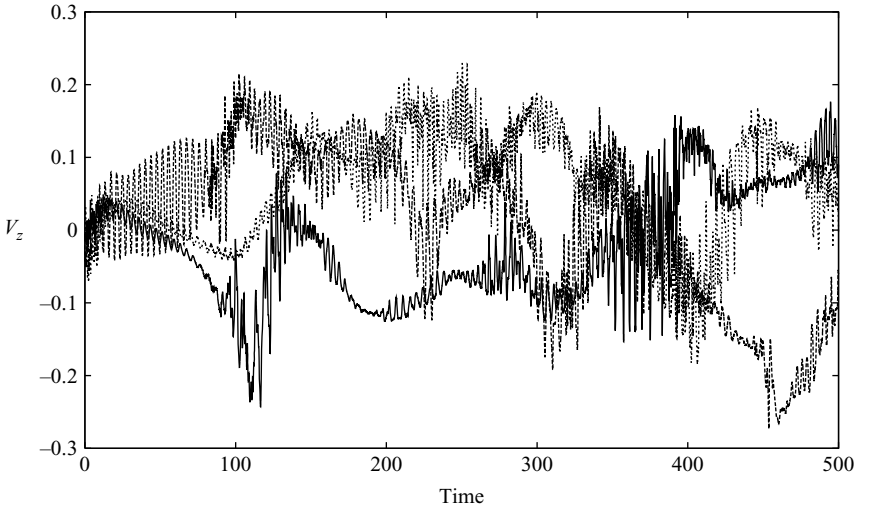

FIGURE 2. Axial perturbation velocity signal at three different locations in the pipe: ($s = 0.66, \theta = 0, z = 0$), ($s = 0.92, \theta = 0, z = 0$) and ($s = 0.76, \theta = 0, z = 0.5D$). The signal is taken from the edge trajectory in § 3.1. Dotted arrows indicate where the velocity signal shows approximate recurrences.

function

$$r_i(t > t_i) := \frac{|\boldsymbol{X}^{-\Delta z, -\Delta\theta}(t) - \boldsymbol{X}(t_i)|}{|\boldsymbol{X}(t_i)|}, \tag{3.2}$$

where Δz is a distance by which the state $\boldsymbol{X}(t)$ is shifted back in z for comparison. We chose $\Delta z = L$ so that a value of $r_i(t) = 0$ for some $t > t_i$ means that the flow in the pipe is *exactly* the flow at time t_i. In this case, $\boldsymbol{X}(t_i)$ lies on a periodic orbit of the system with the time interval $t - t_i$ being a multiple of the period (for $\Delta z \neq 0$, a vanishing residual would indicate a *relative* periodic orbit). For the ease of calculation, most of the time we chose to neglect the possibility of recurrence occurring after a shift in the azimuthal direction θ, and therefore $\Delta\theta = 0$ was imposed. Typical plots of $r_i(t)$ starting from different values of t_i are displayed in figure 3. Every function r_i attains a smallest local minimum which is defined as

$$r_{\min}(t_i) := \min_{t > t_i} \left\{ r_i(t) : \frac{\partial r_i}{\partial t} = 0 \right\}. \tag{3.3}$$

Figure 4 shows how $r_{\min}$ varies with the starting point. Phases for which $r_{\min}$ is small (from experience below 0.1) may be interpreted as approximate approaches to periodic orbits of the system by the edge trajectory. The alternating pattern of maxima and minima in $r_{\min}$ is then the signature of a repellor – a set of states which attract trajectories before ultimately repelling them away. For hyperbolic dynamical systems, trajectories are attracted towards one of these states along their stable manifold and ejected away along their unstable manifold (see the sketch in figure 5). For the parameters here, six dips in the $r_{\min}$-profile are suggestive of six approaches, denoted respectively by A1, B1, C1, D1, E1, F1. Parts of the trajectory linking one state to the next (e.g. A1 → B1 or D1 → E1) may be located in the vicinity of heteroclinic connections between the two states, should such a connection exist, or a relative homoclinic connection for two successive states which are the same but for a shift. The notion of 'vicinity' depends on the choice of the norm in phase space. Here, a

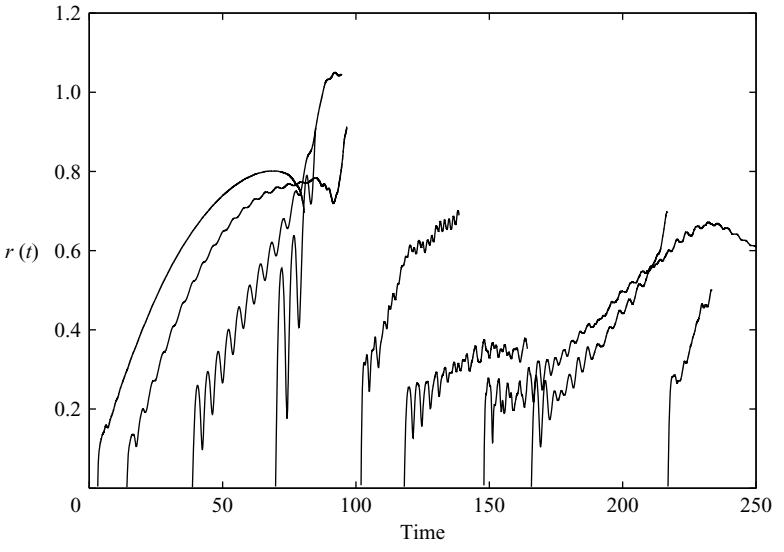

FIGURE 3. Typical profiles of the residual function $r(t)$ starting from snapshots of the edge trajectory of § 3.1. The subscript i has been suppressed (time in units of D/U).

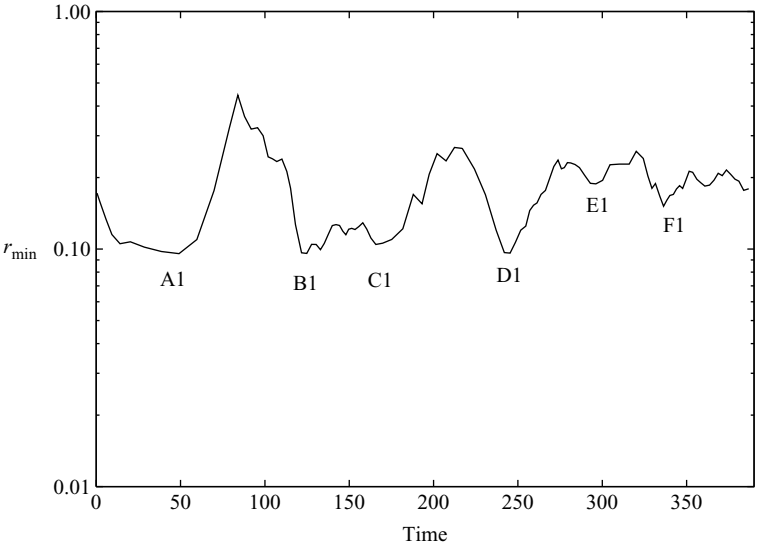

FIGURE 4. Recurrence signal for the edge trajectory of § 3.1 (for definition of $r_{\min}$ see text) against time in D/U; $(\alpha, Re, m_0) = (0.625, 2875, 1)$.

pragmatic approach is adopted: we use the expression '$\boldsymbol{X}$ is close to a periodic orbit Y' to mean that the Newton–Krylov algorithm converges to the periodic orbit Y starting with the initial guess $\boldsymbol{X}$.

3.3. *Exact coherent structures in* Σ

We now analyse the neighbourhood of the points $\boldsymbol{X}(t_i)$ yielding a low value of $r_{\min}$ looking for exact recurrent states for which $r_{\min}$ exactly vanishes. Starting from such initial guesses, the Newton–Krylov algorithm defined in § 2.3 was used to further minimize $r_{\min}$. Of the six different starting guesses A to F introduced in the previous

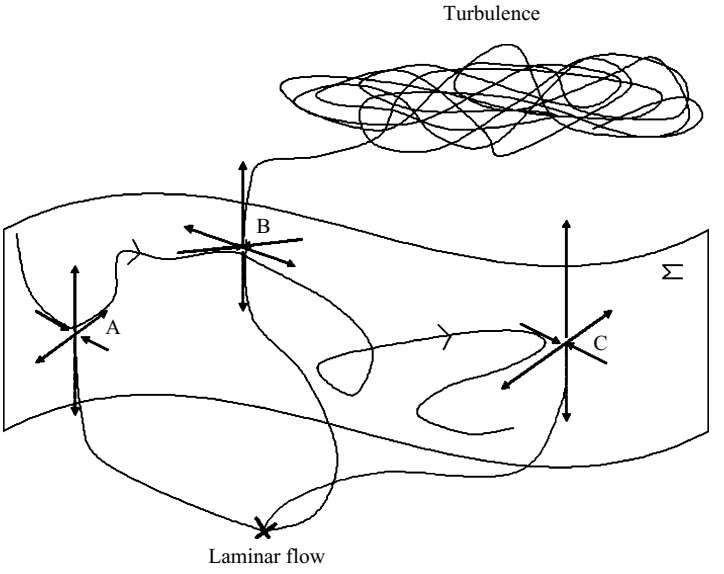

FIGURE 5. Schematic view of phase space. The surface Σ separates initial conditions which relaminarize from those which become turbulent. An edge trajectory visiting three states A, B and C is shown schematically. The dynamics on the manifolds transverse to Σ are shown by trajectory diverging towards either the laminar state or the turbulent state.

subsection, excellent convergence was obtained in the cases A1, B1, D1 and F1, with $r_{\min}$ being reduced down to $O(10^{-11})$. The converged states are labelled respectively A1_0.625, B1_0.625, D1_0.625 and F1_0.625 in order to distinguish them from the starting points A1, ..., F1, and to indicate the parameter α. The cases C1 and E1 displayed only partial convergence to respectively $O(10^{-3})$ and $O(10^{-2})$ and it is not possible to say if there really are zeros of $r_{\min}$ in this neighbourhood. Despite 'globalization' improvements to the Newton–Krylov algorithm to improve convergence, sample starting guesses away from the candidates A, ..., F failed to converge. The converged states A1_0.625, B1_0.625, D1_0.625 and F1_0.625 all correspond to travelling wave solutions. Close inspection of their spatial structure and dynamics shows that they are, in fact, the *same* travelling wave solution modulo a shift in the azimuthal direction: see figure 6. This state corresponds exactly to the 'asymmetric' TW identified in Pringle & Kerswell (2007), whose z-averaged velocity field is strongly reminiscent of the chaotic state calculated by Schneider *et al.* (2007*b*). This resemblance has also been noted by Mellibovsky & Meseguer (2007), who used a different approach to infer the significance of this same asymmetric TW. Interestingly, the present study at these parameter values did not find evidence of states with higher rotational symmetry in spite of the fact that such TWs are known to be embedded in the edge (see figure 4 of Kerswell & Tutty 2007).

The search for recurrent states described above was initially undertaken with $\Delta\theta = 0$ disallowing azimuthal propagation of the recurrent patterns. In the case A1, we experimented with allowing $\Delta\theta$ to be updated by the Newton–Raphson scheme. This involved solving an additional equation $\partial g/\partial\Delta\theta = 0$ (Viswanath 2007). Using Newton–Krylov with the same starting guess A1 but allowing the shift $\Delta\theta$ to be updated, produced convergence to another state A′_0.625 which is distinct from A1_0.625. This state, despite a velocity profile very analogous to that of A1_0.625,

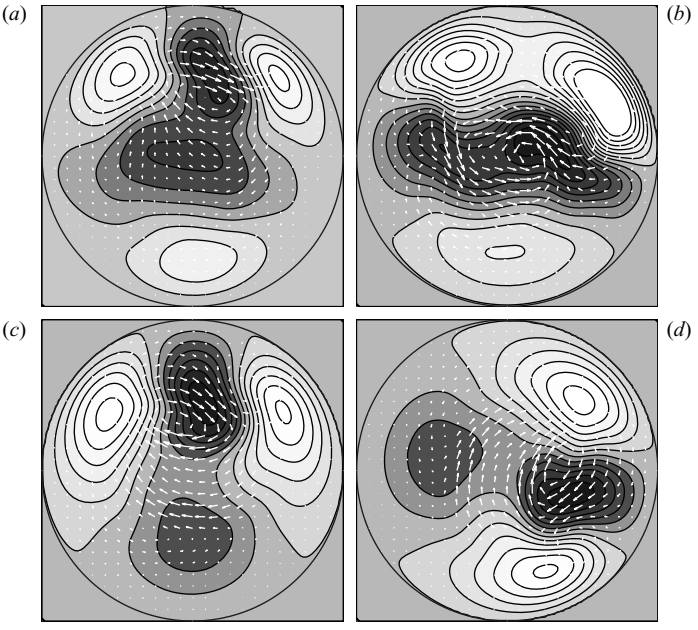

FIGURE 6. Starting guesses for the Newton–Krylov algorithm – (*a*) A1, (*b*) B1 and converged states – (*c*) A1_0.625, (*d*) B1_0.625) – on the edge trajectory described in § 3.2. Each subfigure represents a snapshot across the pipe. Contours indicate the axial velocity difference from the underlying laminar flow (light/dark indicating faster/slower moving fluid) and the arrows represent the cross-stream velocity (length proportional to speed). Maximum norm of the (u, v) cross-velocity is $0.0128U$ and the axial velocity differential w is in the range $\pm 0.17U$. The TWs A1_0.625 and B1_0.625 are exactly the same state modulo an azimuthal shift.

rotates by an angle $\Delta\theta = -0.32$ degrees after travelling one pipe length. This situation is reminiscent of the bifurcation diagram obtained by Pringle & Kerswell (2007) for the asymmetric TW (though here Re is much higher): for a given Reynolds number, a branch of solutions with helicity is connected to the mirror-symmetric branch, and intersects the non-helical subspace twice. The solutions at the crossing points are non-helical but nevertheless possess a rotational propagation speed $c_\theta \neq 0$, like our solution A′_0.625. The fact that such a solution has been found here could be explained by the fact that the numerical code used does not allow helicity, hence the Newton–Krylov algorithm has no choice but to look for the intersection of the helical branch with a non-helical subspace. However, other attempts to find exact recurrent patterns with rotation invariably converged back to a non-rotating ($\Delta\theta = 0$) TW.

3.4. *Search for heteroclinic connections*

The results so far indicate the possible existence of heteroclinic trajectories linking the exact states found. When the two consecutively visited states are the same modulo a shift in the azimuthal direction, 'relative' homoclinic connection is a more appropriate term. In an attempt to find further evidence for such connections, a series of initial conditions sampling the unstable manifold of a TW were explored. The asymmetric travelling wave of Pringle & Kerswell (2007) was chosen (i.e. A1_0.625) with the parameters $(\alpha, Re, m_0) = (0.625, 2875, 1)$ and orientated so that it was $\boldsymbol{S}$-symmetric about the $\theta = 0$ plane. In the corresponding $\boldsymbol{S}$-symmetric subspace, the solution has exactly two unstable eigendirections, denoted by $\boldsymbol{e}_1$ and $\boldsymbol{e}_2$, $\boldsymbol{e}_1$ being the most unstable one (there are no unstable directions in the dual space of $\boldsymbol{S}$-*anti* symmetric

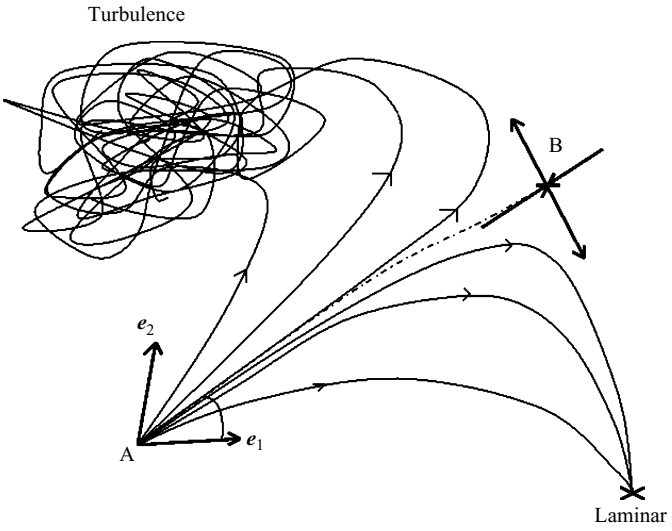

FIGURE 7. A sketch of the heteroclinic connnection joining two saddle points A and B; $\boldsymbol{e}_1$ and $\boldsymbol{e}_2$ are the two unstable eigendirections of A, used for shooting by varying the shooting angle, in order to optimize the approach to B.

perturbations). These two vectors were normalized to have unit energy and an initial condition was defined as

$$\boldsymbol{X}(0) = \boldsymbol{X}_{TW} + \epsilon\,(\cos\phi\,\boldsymbol{e}_1 + \sin\phi\,\boldsymbol{e}_2)\,. \tag{3.4}$$

Here, ϵ is a positive parameter chosen small enough that $\boldsymbol{X}(0)$ is effectively in the unstable manifold of $\boldsymbol{X}_{TW}$ ($\epsilon = 10^{-2}$ suffices). The angle ϕ defines a plane spanned by $\boldsymbol{e}_1$ and $\boldsymbol{e}_2$ and vanishes in the direction of $\boldsymbol{e}_1$. For some values of the angle ϕ, the trajectory starting at $\boldsymbol{X}(0)$ returns to the laminar state, whereas for others it becomes turbulent. Boundary values of ϕ between these two behaviours lead to intermediate dynamics, demonstrating that $\boldsymbol{X}_{TW}$ sits on the edge Σ. In all cases the trajectory starts in the $\boldsymbol{S}$-symmetric subspace, but after a finite time this symmetry is broken by numerical noise. A bisection method is used to determine (to machine precision) an angle ϕ for which the trajectory neither evolves to the laminar or turbulent state (see figure 7 for a sketch of the method). The energy contained in the axially dependent modes is displayed in figure 8 and the residual function $r_{\min}(t)$ in figure 9. These show that $r_{\min}$ increases exponentially but the energy changes little until $t \sim 150D/U$. After this linear regime, $r_{\min}$ continues to increase, then drops to a local minimum value of 0.09 at $t \sim 250D/U$ before increasing again. When the state at the local minimum (B4 in figure 9) was used as a starting point for the Newton–Krylov algorithm, $r_{\min}$ smoothly decreased down to $O(10^{-11})$. The exact solution found was the asymmetric travelling wave again, but now shifted by an angle of 51.56°. On the basis that the Newton–Krylov method usually needs to be in the vicinity of an exact solution to converge to it, this suggests the existence of a relative homoclinic connection near the computed trajectory. Collecting firmer evidence is difficult unless the dynamics is further restricted. Recently, significant progress has been made along these lines in plane Couette flow by Gibson, Halcrow & Cvitanović (2008) who have demonstrated the existence of a heteroclinic connection between two steady solutions on Σ for a minimal flow unit.

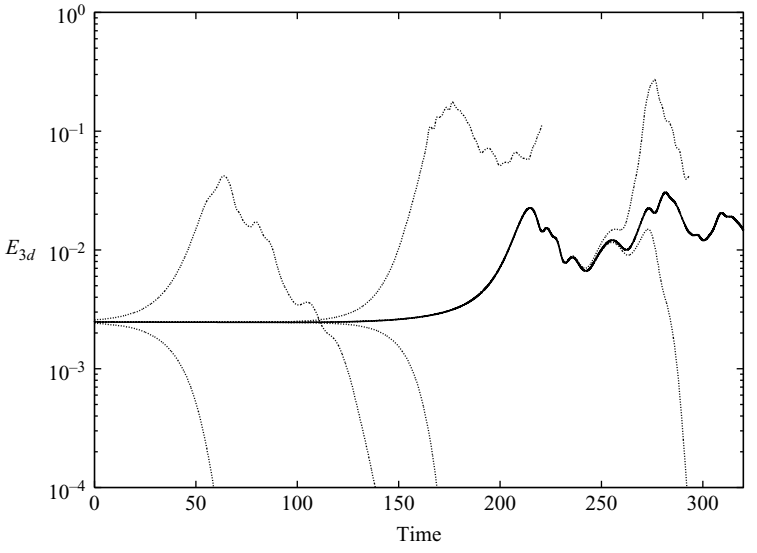

FIGURE 8. Energy contained in the axially dependent modes for $Re = 2875$, $m_0 = 1$, $\alpha = 0.625$. The thick line indicates the edge trajectory and the thinner lines nearby trajectories which either relaminarize (energy decreases) or become turbulent (energy increases to a higher level). Time is in units of D/U.

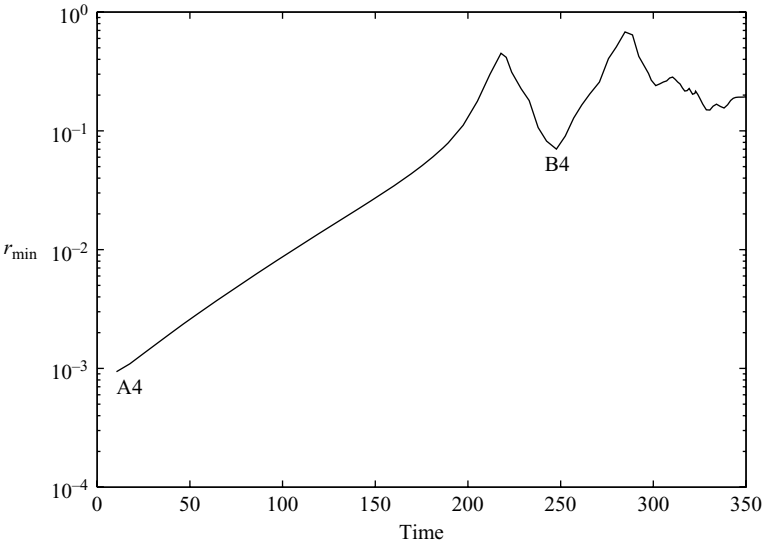

FIGURE 9. Recurrence signal for the heteroclinic connection of § 3.4 versus time (in D/U); $(\alpha, Re, m_0) = (0.625, 2875, 1)$.

3.5. Σ *under* $\boldsymbol{R}_2$*-symmetry*

The technique developed above to identify recurrent states in the edge can also equally be applied to the dynamics within a symmetry subspace. Restricting the flow to be $\boldsymbol{R}_m$-symmetric, for example, improves the possibility of an edge trajectory coming close to some of the $\boldsymbol{R}_m$-symmetric lower-branch TWs found to be in the edge by Kerswell &

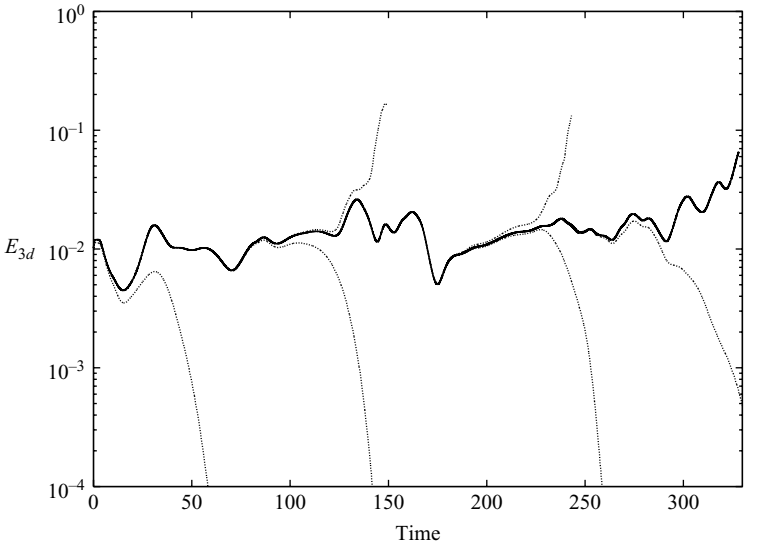

FIGURE 10. Energy contained in the axially dependent modes on the edge for $(\alpha, Re, m_0) = (0.625, 2875, 2)$. The thick line indicates the edge trajectory and the thinner lines nearby trajectories which either relaminarize (energy decreases) or become turbulent (energy increases to a higher level). Time is in units of D/U.

Tutty (2007). There is also, of course, the possibility of discovering unknown branches of TWs. Attention was restricted to the $\boldsymbol{R}_2$-symmetric subspace by setting $m_0 = 2$ in the flow representation (2.4). At $Re = 2875$, $\alpha = 0.625$ and resolution (30, 15, 15), an apparently chaotic edge trajectory was followed for $O(500D/U)$ during which 5 different phases of relative recurrence – labelled A2, B2, C2, D2 and E2 in chronological order – were detected. Interestingly, this edge trajectory, although seemingly chaotic, is much smoother than the corresponding (same Re and α) edge trajectory for $m_0 = 1$: compare figures 1 and 10. Of the 5 initial conditions for a Newton–Krylov search, $r_{\min}$ only converged to $O(10^{-11})$ for D2 and E2 ($r_{\min}$ for A2, B2 and C2 stagnated at $O(10^{-3})$).

The exact recurrence states found, D2_0.625 and E2_0.625 (see figure 11), correspond to two new types of travelling wave branches distinct from those originally reported in Faisst & Eckhardt (2003) and Wedin & Kerswell (2004). D2_0.625 is especially interesting as it is the first TW found in pipe flow which is *not* $\boldsymbol{S}$-symmetric. It does, however, possess a mirror symmetry

$$\boldsymbol{Z}_\psi : (u, v, w, p)(s, \phi, z) \to (u, -v, w, p)(s, 2\psi - \phi, z) \tag{3.5}$$

where $\psi \approx 45^\circ$ (or equivalently $\approx -45^\circ$ because of the imposed $\boldsymbol{R}_2$-symmetry) for the snapshot shown in figure 11. In contrast, E2_0.625 has three symmetries: two unimposed – $\boldsymbol{S}$ and $\boldsymbol{Z}_{\pm\pi/4}$ (where $\phi = 0$ defines the plane of shift-and-reflect symmetry) – and one imposed – $\boldsymbol{R}_2$. E2_0.625 is actually one member of a whole new class of *highly* symmetric TWs which have subsequently been uncovered (the N-class: see Pringle *et al.* 2008). These new waves are significant because they appear much earlier in Re than the originally discovered TWs (Faisst & Eckhardt 2003; Wedin & Kerswell 2004) and their upper-branch solutions look more highly nonlinear.

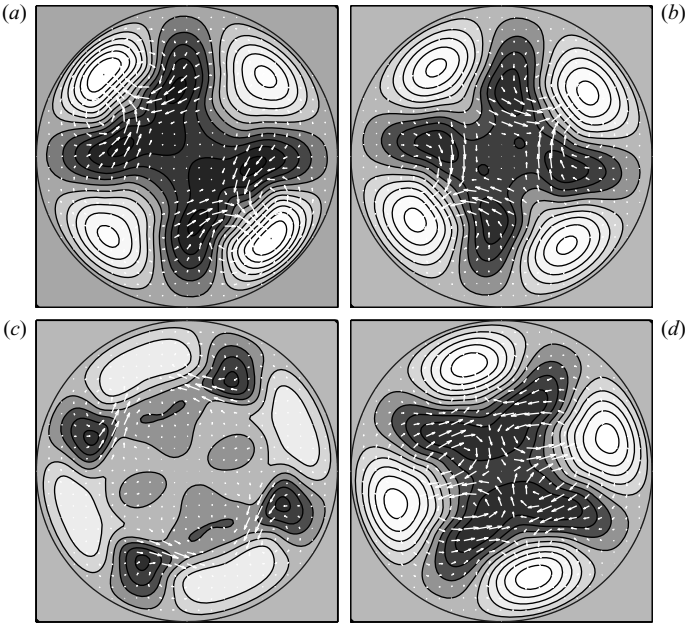

FIGURE 11. Converged states D2_0.625 (*a*), E2_0.625 (*b*), A3_1.25 (*c*) and C3_1.25 (*d*). Contours indicate the axial velocity difference from the underlying laminar flow (light/dark indicating faster/slower moving fluid) and the arrows represent the cross-stream velocity (length proportional to speed). Across the four snapshots, the maximum cross-stream speed is $0.0143U$, and the axial velocity perturbation w is in the range $\pm 0.17U$.

3.6. *Local relative attractors within the* $\boldsymbol{R}_2$*-symmetric subspace*

In this subsection, the flow is again restricted to be $\boldsymbol{R}_2$-symmetric but the pipe is halved in length ($\alpha = 1.25$ so $L \approx 2.5D$) and Re reduced to 2400 (resolution is (50, 20, 8)). At these settings, Kerswell & Tutty (2007) identified a lower-branch TW – 2*b*_1.25 in their nomenclature – which was on the edge with only one unstable direction normal to it. This TW is therefore a local attractor for trajectories confined to the edge. A leading question is whether it is also a global attractor on the edge.

A starting point was randomly chosen along a turbulent trajectory, and an edge trajectory generated for $500D/U$ using the method described above. The energy signal is displayed in figure 12 and the corresponding recurrence signal $r_{\min}(t)$ is displayed in figure 13. Two successive dips in $r_{\min}$ can be seen at times $50D/U$ and $90D/U$ later corresponding to inexact recurrences labelled, respectively, A3 and B3. When used to initialize a Newton–Krylov search, both led to a value of $O(10^{-11})$ for $r_{\min}$. The two converged exact states correspond to one unique travelling wave solution, differing only by a small shift in the azimuthal direction of less than 4 degrees. As a result, we label only the first A3_1.25: see figure 11. The TW A3_1.25 has all the same symmetries as E2_0.625 but possesses a distinctly different structure consisting of 4 low-speed streaks near the walls separated by 4 high-speed streaks. Four other high-speed streaks of lesser amplitude and smaller size, and with a much more steady structure, can be found closer to the pipe axis. This new TW thus has a richer structure than the $\boldsymbol{R}_2$ branch of solutions found in Faisst & Eckhardt (2003) and Wedin & Kerswell (2004). Just as for E2_0.625, subsequent investigations have revealed that

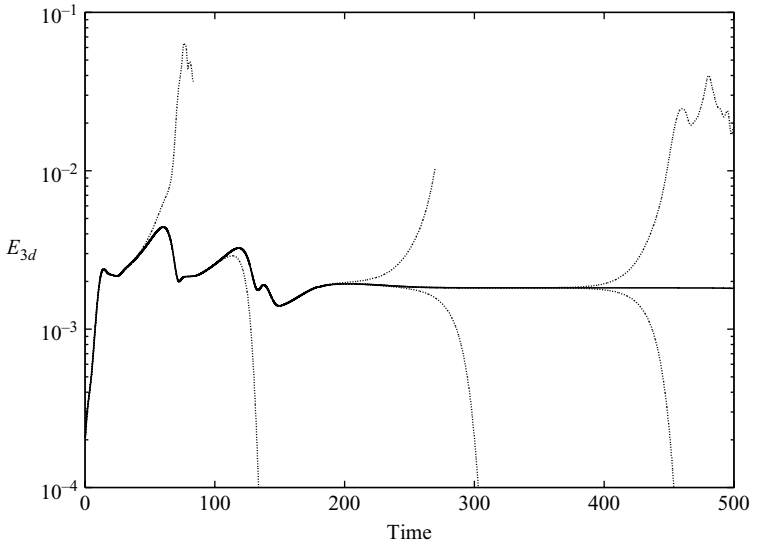

FIGURE 12. Energy contained in the axially dependent modes for $(\alpha, Re, m_0) = (1.25, 2400, 2)$. The thick line indicates the edge trajectory and the thinner lines nearby trajectories which either relaminarize (energy decrease) or become turbulent (energy increases to a higher level). Time is in units of D/U.

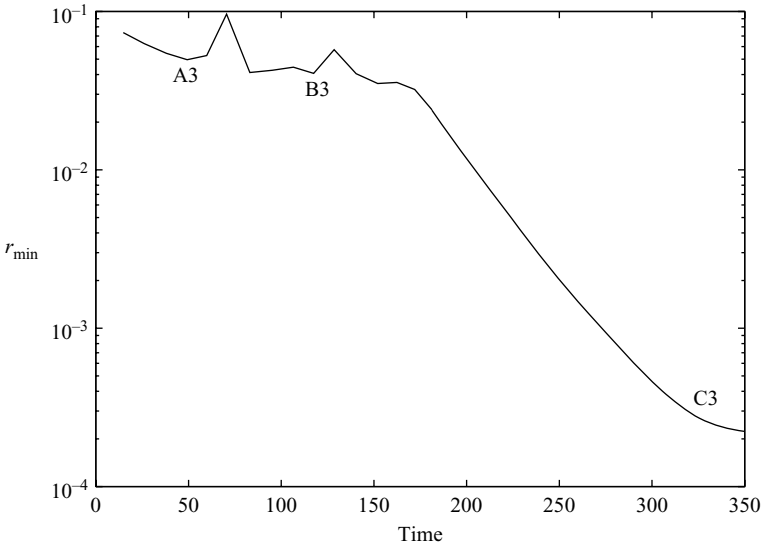

FIGURE 13. Recurrence signal for the attracting state of § 3.5 versus time expressed in D/U units; $(\alpha, Re, m_0) = (1.25, 2400, 2)$.

A3_1.25 is but one member of another highly symmetric class of TWs (the M-class: Pringle *et al.* 2008) characterized by this distinctive double-layer structure.

After a time $200D/U$, the energy of the edge trajectory reaches a constant plateau and the value of $r_{\min}$ decreases exponentially to $O(10^{-4})$ by $300D/U$. This indicates that the trajectory is converging to an end state. Newton–Krylov was used to accelerate the convergence of the trajectory by taking the state at $300D/U$ and reducing $r_{\min}$ to

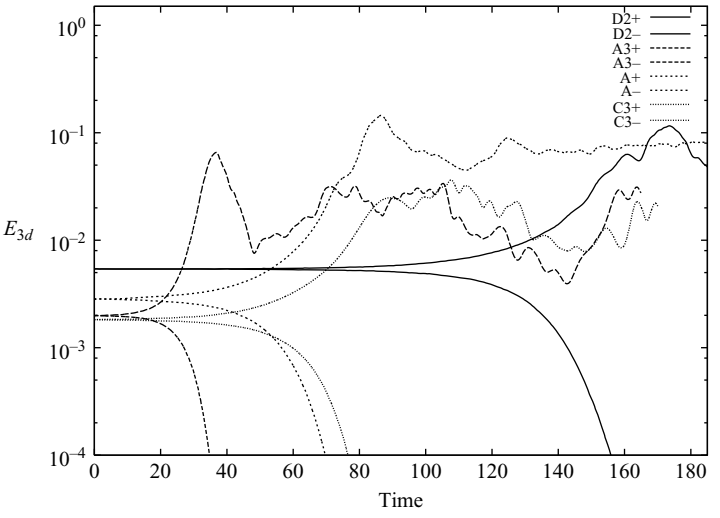

FIGURE 14. Diverging trajectories demonstrating the 'edge credentials' of the new TWs found here. Two typical trajectories starting close to each TW are shown with one decaying down smoothly to the laminar state ($E_{3d} = 0$) and another increasing up to the turbulent state. D2 represents D2_0.625, A3 is A3_1.25, A is A1_0.625 and C3 is C3_1.25, with $\pm$ used to distinguish the starting perturbation.

$O(10^{-11})$. The spatial structure of the initial and final state of this procedure, however, is indistinguishable. The final state is another travelling wave solution, C3_1.25 (see figure 11), distinct from 2*b*_1.25 of Kerswell & Tutty (2007). Stability analysis of C3_1.25 reveals only one unstable direction, which has to be normal to the edge (see Pringle *et al.* 2008 for details). Hence C3_1.25 is an attractor in the edge, and both C3_1.25 and 2*b*_1.25 can only be local attractors there. Closer examination of E2_0.625 and C3_1.25, which look very similar, reveals that they are members of the same TW family, distinguished only by their different wavelengths.

3.7. *Travelling waves on the edge*

There is no guarantee that starting guesses taken from the edge for the Newton–Krylov method will converge to states also on the edge. The calculations of § 3.4 have, however, demonstrated this for A1_0.625 (the asymmetric TW) thereby confirming earlier speculation (Schneider *et al.* 2007*b*; Pringle & Kerswell 2007). To check this explicitly for the other TWs found here, each was taken as an initial condition with various very small perturbations added to start a series of runs. In all cases, two contrasting behaviours were evident: one perturbation could be found which led to relaminarization, while another led to a turbulent episode: see figure 14. This confirms that all the TWs found here are on the laminar–turbulent boundary for the particular parameter settings tested (shown in table 1).

4. Discussion

A summary of the main findings of this investigation is listed below.

(i) The laminar–turbulent boundary Σ in a short pipe seems to have a chaotic attractor, as observed by Schneider *et al.* (2007*b*).

TW	m_0	Re	C	c_θ	Status
A1_0.625	1	2875	1.55494	0	known
A′_0.625	1	2875	1.51956	$-1.704.10^{-3}$	new
D2_0.625	2	2875	1.53382	0	new
A3_1.25	2	2400	1.23818	0	new
C3_1.25	2	2400	1.55064	0	new

TABLE 1. Parameters, axial propagation speed C (in units of U) and azimuthal propagation speed c_θ in rad U/D and status of all travelling wave solutions found in this paper (E2_0.625 is in the same TW family as C3_1.25 and hence not listed separately).

(ii) Although Σ has many unstable lower-branch TWs embedded within it (e.g. Kerswell & Tutty 2007), only one – the asymmetric TW of Pringle & Kerswell (2007) (and rotated derivatives of it) – was approached by edge trajectories studied here.

(iii) A new asymmetric TW which has a small but finite azimuthal phase speed has been discovered.

(iv) Some evidence was gathered for a 'relative' homoclinic connection between the asymmetric TW and the same wave with a different orientation.

(v) Calculations within a $\boldsymbol{R}_2$-symmetric subspace have revealed new branches of $\boldsymbol{R}_2$-symmetric TW solutions. One (D2_0.625) is the first TW found *not* to be shift-and-reflect symmetric in pipe flow, while the others are members of new classes of *highly* symmetric TWs (Pringle *et al.* 2008).

(vi) The laminar–turbulent boundary restricted to $\boldsymbol{R}_2$-symmetry has at least two simple local attractors in the form of TWs at $Re = 2400$.

Our numerical experiments have shed some light on the dynamical structure of Σ in pipe flow. When no symmetry is imposed, and the pipe is approximately $5D$ long ($\alpha = 0.625$), trajectories which neither relaminarize nor become turbulent all look chaotic and visit some exact recurrent states in a transient manner. In all cases studied, these exact solutions appear to be specifically the asymmetric TWs found by Pringle & Kerswell (2007), even though many other lower-branch TWs are embedded in Σ (Kerswell & Tutty 2007). No RPOs were found, even though the numerical method was sufficiently general to find them, in addition to TWs. Whether this is because the RPOs are rarely visited or just more difficult to isolate is unclear. It is tempting to conclude that chaos on the edge of pipe flow is structured around a set of unstable saddle points (the TWs) linked together by heteroclinic or sometimes relative homoclinic connections. An approximation to such a connection has been shown in § 3.4. The resulting dynamical structure is likely to be a heteroclinic (or homoclinic) tangle, an efficient mechanism to produce chaotic trajectories in phase space with the set of TWs acting as a skeleton of the tangle. Seen from this point of view, transition to turbulence from a given initial condition depends on the position of the initial state, in phase space, relative to the stable manifold of each exact state embedded in Σ. When a trajectory approaches a travelling wave solution belonging to Σ, its relative position to the boundary determines on which side of the edge the trajectory escapes, resulting in either relaminarization or a turbulent transient (see sketch in figure 5).

When the flow is artificially restricted to be $\boldsymbol{R}_2$-symmetric at $Re = 2875$, the trajectory remains chaotic wandering sufficiently close to *distinct* TW states (D2_0.625 and

E2_0.625) to be captured by the Newton–Krylov scheme. By halving the pipe length to $L \approx 2.5D$ and reducing Re to 2400, multiple local attractors appear in Σ. A randomly started trajectory, after a chaotic transient and approaches to states A3_1.25 and B3_1.25, is attracted towards the TW solution C3_1.25. The fundamental difference between C3_1.25 and all the other states mentioned so far lies in the number of unstable eigenvalues. When a TW has two or more unstable eigenvalues in a given subspace, the dimension of the intersection between its unstable manifold and the hypersurface Σ is reduced by one but remains at least one. Hence such a state remains a saddle point on Σ: edge trajectories enter its vicinity along its stable manifold and escape along the unstable manifold. In contrast, when a state has only one unstable direction, this is necessarily normal to Σ, so that the state becomes an attractor for dynamics restricted to the edge (a relative attractor). We have shown that C3_1.25 is one such TW, but there is at least one other, 2b_1.25 of Kerswell & Tutty (2007). Therefore we expect both these two states to be only *local* attractors on Σ rather than global ones. In the cases of plane Poiseuille and Couette flow, a lower-branch solution exists which has only one unstable direction and is therefore a relative attractor (Toh & Itano 1999; Itano & Toh 2001; Wang *et al.* 2007; Schneider *et al.* 2008; Viswanath 2008). Pipe flow is different as TWs all seem to have at least two unstable directions when there is no imposed discrete rotational symmetry. For example, the 2b_1.25 TW has one harmonic ($\boldsymbol{R}_2$-symmetric) unstable eigenfunction and one subharmonic (only $\boldsymbol{R}_1$-symmetric) unstable eigenfunction.

While discrete rotational symmetry constraints might appear artificial, they have nevertheless served as a useful device for discovering new exact recurrent solutions (see table 1). The method developed here, based on edge tracking, recurrence analysis and use of a Newton–Krylov algorithm, is a general approach for finding new exact recurrent solutions in any flow situation possessing subcritical behaviour. Importantly, the present method naturally selects the states that are most likely to be visited and does not presuppose anything about their spatial structure (modulo the symmetries imposed on the flow). The use of the scalar function $r_{\min}$, coupled with a Newton–Krylov solver, can also be used to search for more complex solutions such as relative periodic orbits, whether located on the laminar–turbulent boundary or embedded in fully developed turbulence. This is currently underway.

Many open questions remain regarding Σ in pipe flow. Is Σ really a hypersurface or can it have a more fractal structure? Why does the flow keep approaching the asymmetric TW or rotations of it, and not any of the other lower-branch TWs known to exist within the same parameter range? Finally, what are the properties of Σ for longer pipes, where localized turbulent 'puffs' structures exist? Preliminary work for the extended pipe in a reduced model has already revealed an interesting localized structure as the attracting state (Willis & Kerswell 2008*b*).

We would like to thank C. Pringle for helping with the velocity profiles of the TW solutions and B. Eckhardt for stimulating discussions about this topic. Y. D. was supported by a Marie-Curie Intra-European Fellowship (grant number MEIF-CT-2006-024627) and A. W. by the EPSRC (grant number GR/S76144/01).

REFERENCES

Brown, P. N. & Saad, Y. 1990 Hybrid Krylov methods for nonlinear systems of equations. *SIAM J. Sci. Statist. Comput.* **11**, 450–481.

Dennis, J. E., Jr & Schnabel, R. E. 1995 *Numerical Methods for Unconstrained Optimization and Nonlinear Equations*. SIAM.

Eisenstat, C. & Walker, H. 1996 Choosing the forcing terms in an inexact Newton method. *SIAM J. Sci. Comput*. **17**, 16–32.

Faisst, H. & Eckhardt, B. 2003 Travelling waves in pipe flow. *Phys. Rev. Lett*. **91**, 224502.

Faisst, H. & Eckhardt, B. 2004 Sensitive dependence on initial conditions in transition to turbulence. *J. Fluid Mech*. **504**, 343–352.

Gibson, J. F., Halcrow, J. & Cvitanović, P. 2008 The geometry of state-space in plane Couette flow. *J. Fluid Mech*. (submitted).

Hagen, G. H. L. 1839 Über die Bewegung des Wassers in engen zylindrischen Rohren. *Poggendorfs Annal. Physik Chemie* **16**, 423.

Hamilton, J. M., Kim, J. & Waleffe, F. 1995 Regeneration mechanisms of near-wall turbulence structures. *J. Fluid Mech*. **287**, 317–348.

Hof, B., van Doorne, C. W. H., Westerweel, J., Nieuwstadt, F. T. M., Faisst, H., Eckhardt, B., Wedin, H., Kerswell, R. R. & Waleffe, F. 2004 Experimental observation of non-linear traveling waves in turbulent pipe flow. *Science* **305**, 1594–1597.

Hof, B., van Doorne, C. W. H., Westerweel, J. & Nieuwstadt, F. T. M. 2005. Transition in pipe flow: the saddle structure on the boundary of turbulence. *Phys. Rev. Lett*. **95**, 214502.

Itano, T. & Toh, S. 2001 The dynamics of bursting process in wall turbulence. *J. Phys. Soc. Japan* **70**, 703–716.

Jiménez, J. & Moin P. 1991 The minimal flow unit in near-wall turbulence. *J. Fluid Mech*. **225**, 213–240.

Joseph, D. D. & Carmi, S. 1969 Stability of Poiseuille flow in pipes, annuli, and channels. *Quart. Appl. Math*. **26**, 575–599.

Kawahara, G. 2005 Laminarization of minimal plane Couette flow: Going beyond the basin of attraction of turbulence. *Phys. Fluids* **17**, 041702.

Kerswell, R. R. 2005 Recent progress in understanding the transition to turbulence in a pipe. *Nonlinearity* **18**, R17–R44.

Kerswell, R. R. & Tutty, O. R. 2007 Recurrence of travelling waves in transitional pipe flow. *J. Fluid Mech*. **584**, 69–102.

Marqués, F. 1990 On boundary conditions for velocity potentials in confined flows: Application to Couette flow. *Phys. Fluids* A 2, 729–737.

Mellibovsky, F. & Meseguer, A. 2007 Pipe flow dynamics on the critical threshold. In *Proc. 15th Intl Couette–Taylor Workshop* (ed. I. Mutabazi), Le Havre, France.

Nagata, M. 1990 Three dimensional finite amplitude solutions in plane Couette flow: Bifurcation from infinity. *J. Fluid Mech*. **217**, 519–527.

Nikitin N. 2007 Spatial periodicity of spatially evolving flows caused by inflow boundary condition. *Phys. Fluids* **19**, 091703.

Peixinho, J. & Mullin, T. 2006 Decay of turbulence in pipe flow. *Phys. Rev. Lett*. **96**, 094501.

Peixinho, J. & Mullin, T. 2007 Finite-amplitude thresholds for transition in pipe flow. *J. Fluid Mech*. **582**, 169–178.

Pfenniger, W. 1961 Transition in the inlet length of tubes at high Reynolds numbers. In *Boundary Layer and Flow Control* (ed. G. V. Lachman), pp. 970–980. Cambridge University Press.

Poiseuille, J. L. M. 1840 Recherches experimentales sur le mouvement des liquides dans les tubes de très petits diamètres. *CR Acad. Sci*. **11**, 961.

Pringle, C. C. T. & Kerswell, R. R. 2007 Asymmetric, helical and mirror-symmetric travelling waves in pipe flow. *Phys. Rev. Lett*. **99**, 074502.

Pringle, C. C. T., Duguet, Y. & Kerswell, R. R. 2008 Highly-symmetric travelling waves in pipe flow. *Phil. Trans. R. Soc*. (submitted).

Priymak, V. G. Miyazaki, T 2004 Direct numerical simulation of equilibrium spatiallly-localized structures in pipe flow. *Phys. Fluids*, **16**, 4221–4234.

Reynolds, O. 1883 An experimental investigation of the circumstances which determine whether the motion of water shall be direct or sinuous and of the law of resistance in parallel channels. *Phil. Trans. R. Soc*. **174**, 935–982.

Saad, Y. & Schultz, M. H. 1986 GMRES: A generalized minimal residual method for solving nonsymmetric linear systems. *SIAM J. Sci. Statist. Comput*. **7**, 856–869.

Schneider, T. M., Eckhardt, B. & Vollmer, J. A. 2007*a* Statistical analysis of coherent structures in transitional pipe flow. *Phys. Rev.* E **75**, 066313.

Schneider, T. M., Eckhardt, B. & Yorke, J. A. 2007*b* Turbulence transition and the edge of chaos in pipe flow. *Phys. Rev. Lett.* **99**, 034502.

Schneider, T. M., Gibson J. F., Lagha, M., De Lillo, F. & Eckhardt, B. 2008 Laminar–turbulent boundary in plane Couette flow. Preprint (http://arxiv.org/abs/0805.1015).

Skufca, J. D., Yorke, J. A. & Eckhardt, B. 2006 Edge of chaos in a parallel shear flow. *Phys. Rev. Lett.* **96**, 174101.

Toh, S. & Itano, T. 1999 Low-dimensional dynamics embedded in a plane Poiseuille flow turbulence: Traveling-wave solution is a saddle point? In *Proc. IUTAM Symp. on Geometry and Statistics of Turbulence* (ed. T. Kambe), Kluwer.

Viswanath, D. 2007 Recurrent motions within plane Couette turbulence. *J. Fluid Mech.* **580**, 339–358.

Viswanath, D. 2008 The dynamics of transition to turbulence in plane Couette. In *Mathematics and Computation: A Contemporary View*. Springer.

Waleffe, F. 1997 On the self-sustaining process in shear flows. *Phys. Fluids* **9**, 883–900.

Waleffe, F. 1998 Three dimensional coherent states in plane shear flows. *Phys. Rev. Lett.* **81**, 4140–4143.

Waleffe, F. 2001 Exact coherent structures in channel flow. *J. Fluid Mech.* **435**, 93–102.

Waleffe, F. 2003 Homotopy of exact coherent structures in plane shear flows. *Phys. Fluids* **15** 1517–1534.

Wang, J., Gibson, J. & Waleffe, F. 2007 Lower branch coherent states in shear flows: Transition and control. *Phys. Rev. Lett.* **98**, 204501.

Wedin, H. & Kerswell, R. R. 2004 Exact coherent structures in pipe flow: Travelling wave solutions. *J. Fluid Mech.* **508**, 333–371.

Willis, A. P. & Kerswell, R. R. 2007 Critical behaviour in the relaminarisation of localised turbulence in pipe flow. *Phys. Rev. Lett.* **98**, 14501.

Willis, A. P. & Kerswell, R. R. 2008*a* Coherent structures in local and global pipe turbulence. *Phys. Rev. Lett.* **100**, 124501.

Willis, A. P. & Kerswell, R. R. 2008*b* Turbulent dynamics of pipe flow captured in a reduced model: Puff relaminarisation and localised 'edge' states. *J. Fluid Mech.* (submitted).

Wygnanski, I. J. & Champagne, F. H. 1973 On transition in a pipe. Part 1. The origin of puffs and slugs and the flow in a turbulent slug. *J. Fluid Mech.* **59**, 281.